PHYSICS

Experimental measurement of the intrinsic excitonic wave function

Michael K. L. Man[1†], Julien Madéo[1†], Chakradhar Sahoo[1,2], Kaichen Xie[3], Marshall Campbell[4], Vivek Pareek[1], Arka Karmakar[1], E Laine Wong[1‡], Abdullah Al-Mahboob[1], Nicholas S. Chan[1], David R. Bacon[1], Xing Zhu[1], Mohamed M. M. Abdelrasoul[1], Xiaoqin Li[4], Tony F. Heinz[5,6], Felipe H. da Jornada[7], Ting Cao[3,5], Keshav M. Dani[1]*

An exciton, a two-body composite quasiparticle formed of an electron and hole, is a fundamental optical excitation in condensed matter systems. Since its discovery nearly a century ago, a measurement of the excitonic wave function has remained beyond experimental reach. Here, we directly image the excitonic wave function in reciprocal space by measuring the momentum distribution of electrons photoemitted from excitons in monolayer tungsten diselenide. By transforming to real space, we obtain a visual of the distribution of the electron around the hole in an exciton. Further, by also resolving the energy coordinate, we confirm the elusive theoretical prediction that the photoemitted electron exhibits an inverted energy-momentum dispersion relationship reflecting the valence band where the partner hole remains, rather than that of conduction band states of the electron.

INTRODUCTION

In the 1930s, pioneering work by Frenkel (*1*), Wannier (*2*), and others (*3*, *4*) elucidated the presence of optically excited states at energies lying in the forbidden bandgap region of insulators and semiconductors. These states, called excitons, could not be described within a single-particle picture but arose as correlated bound states between a photoexcited electron in the conduction band and the hole left behind in the valence band (VB). As neutral composite quasiparticles of oppositely charged fermions, excitons exhibit different quantum statistics and respond differently to external fields compared to their constituent free carriers. Over the ensuing century, these differences have had inevitable consequences for various condensed matter systems, giving rise to phenomena such as Bose-Einstein condensation (*5*–*7*) and excitonic insulators (*8*) and affecting the performance of photovoltaics (*9*, *10*), light-emitted diodes (*11*, *12*), and other optoelectronic devices (*13*).

As in the case of other two-body systems, the fundamental theoretical description of excitons is naturally formulated in terms of the relative electron-hole coordinates, particularly for the Wannier-type excitons, where electron-hole separation extends over many lattice sites (*14*, *15*). These descriptions, constituting the excitonic wave function in real space, analogous to the well-known wave functions describing the hydrogen atom, directly define the exciton's size and shape. The excitonic wave function can also be described in momentum space, which dictates its ability to interact with light, phonons, plasmons, and other quasiparticles through momentum conservation (*16*). However, since their discovery nearly a century ago, measuring the excitonic wave function, whether in real or reciprocal space, has not been possible (*17*). This is, in part, not only due to the small binding energy and finite lifetimes of excitons in most semiconductor systems but also due to limitations in available experimental techniques. Optical techniques provide precise spectroscopic information about the exciton but do not access the momentum coordinates of the constituent electrons and holes, while techniques such as scanning tunneling microscopy and transmission electron microscopy with very high spatial resolution cannot measure the relative distance between the delocalized electrons and holes in extended systems.

Over the past decade, the discovery of robust excitons in two-dimensional (2D) systems (*18*–*20*) and advances in space-, time-, and angle-resolved photoemission spectroscopy (ARPES) techniques (*21*–*24*) have created unprecedented opportunities in this regard. Analogous to collider experiments of high-energy physics, theoretical studies from the past few years have proposed using a time-resolved (TR)–ARPES framework to dissociate the exciton with a high-energy extreme ultraviolet (XUV) photon and photoemit its constituent electron (*17*, *25*, *26*). Under the right conditions, the momentum of the photoemitted electron corresponds to the relative electron-hole momentum in the exciton and its measured distribution directly reflects the excitonic wave function in reciprocal space (*25*, *27*, *28*). Very recently, a time-resolved ARPES experiment on monolayer (ML) WSe_2, a prototypical 2D semiconductor, validated this approach by resolving excitons with different relative electron-hole momenta, namely, bright and momentum dark excitons (*29*). This successful demonstration immediately raises the tantalizing possibility of imaging the excitonic wave function.

Here, we directly image the exciton wave function in momentum space for the K-valley exciton in ML WSe_2, more precisely, the modulus squared of the excitonic envelope function in reciprocal space. The corresponding real-space wave function, obtained by Fourier transformation, describes the distribution of the electron relative to the hole in the exciton, revealing a radius of 1.4 nm that extends over many lattice sites. By energy resolving the momentum distribution, we also observe the decades old prediction (*23*, *28*, *30*)

[1]Femtosecond Spectroscopy Unit, Okinawa Instittute of Science and Technology Graduate University, Onna, Okinawa, Japan 904 0495. [2]School of Physics, University of Hyderabad, Gachibowli, Hyderabad, 500046 Telangana, India. [3]Department of Materials Science and Engineering, University of Washington, Seattle, WA 98195, USA. [4]Physics Department, Center for Complex Quantum System, The University of Texas at Austin, Austin, TX 78712, USA. [5]Department of Applied Physics, Stanford University, Stanford, CA 94305, USA. [6]SLAC National Accelerator Laboratory, Menlo Park, CA 94720, USA. [7]Department of Materials Science and Engineering, Stanford University, Stanford, CA 94305, USA.
*Corresponding author. Email: kmdani@oist.jp
†These authors contributed equally to this work.
‡Present address: Center for Nano Science and Technology, Italian Institute of Technology, 20133 Milan, Italy.

of the anomalous dispersion effect that has been experimentally elusive under different measurement conditions (*30*, *31*): The photoemitted electron mimics the negative energy-momentum dispersion of the VB of the hole, to which it was previously bound in the exciton, rather than the positive dispersion of its own conduction band.

RESULTS

In our study, we examined an exfoliated ML of WSe_2 transferred onto a thin hexagonal boron nitride (hBN) buffer layer supported by a Si substrate (Fig. 1A). The insulating hBN layer provides a clean, flat substrate while also preventing the quenching of the exciton (fig. S1) (*32*). The VB structure of our sample before photoexcitation was measured using an ultrashort (160 fs) probe pulses at a photon energy of 21.7 eV in XUV to photoemit electrons from the sample. All measurements are performed at a sample temperature of 90 K. Figure S2 confirms key features of the band structure of ML WSe_2 before photoexcitation—the VB maximum (VBM) at the K-valley, a splitting of the VB at the K-valley of 0.47 eV due to spin orbit coupling, and the VBM at the Γ-valley situated 0.57 eV lower in energy than the K-valley. A comparison to a theoretical, first-principles GW calculation of the VB shows very good agreement.

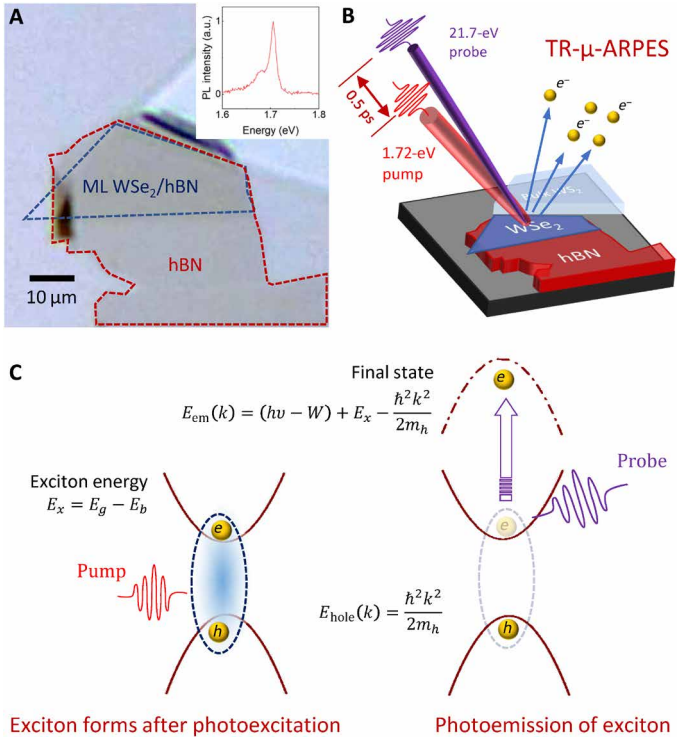

Fig. 1. TR-μ-ARPES experimental scheme and the anomalous dispersion of the photoemitted electron. (**A**) Optical image of the WSe_2/hBN/Si heterostructure, with inset showing photoluminescence spectrum of the ML taken at 90 K. a.u., arbitrary units. (**B**) In our TR-μ-ARPES setup, we resonantly create excitons in the ML WSe_2 using a low-intensity ultrafast pump pulse and photoemit electrons from the excitons using a time-delayed XUV probe pulse. (**C**) As a result of the photoemission process, due to energy and momentum conservation, the energy-momentum dispersion relationship of the photoemitted electron resembles its partner-hole's VB. (see Supplementary Text)

To measure the excitonic states, we resonantly photoexcited the A-exciton transition of the ML WSe_2 at a photon energy of 1.72 eV with a 175-fs linearly polarized pump pulse (Fig. 1B and fig. S1). This created direct excitons with holes and electrons in the K-valley. Subsequently, these excitons scattered into other excitonic states including spin-dark K-K excitons, indirect-bandgap K-K′ excitons and Q-K excitons (*29*), where the two letters denote the valleys of the electron and hole, respectively. To dissociate the excitons and photoemit the constituent electrons, we used a time-delayed XUV probe pulse as above. As expected (*25*–*29*), we observed the below bandgap signal corresponding to electrons photoemitted from the K-valley excitonic states (fig. S2). Further information about the experimental setup for probing the ML WSe_2 band structure before and after photoexcitation, the ensuing exciton dynamics, and the attribution of the signal to the K-valley excitons have been previously reported (*29*).

We now turn our attention to understanding the conditions under which the above measurement provides access to the excitonic wave function. For this, let us consider an exciton in the low-density limit at zero temperature. For such an exciton X, the wave function $|\phi_X\rangle = \sum_{vc\mathbf{k}} A^X_{vc\mathbf{k}} c^\dagger_{c\mathbf{k}} c_{v\mathbf{k}} |0\rangle$ describes the electron-hole bound state, where $|0\rangle$ is the system ground state and $c_{i\mathbf{k}}$ destroys an electron with band index i and wave vector $\mathbf{k}$. The factors $A^X_{vc\mathbf{k}}$ are then expansion coefficients of the exciton in terms of free electron-hole interband pairs, which can be interpreted as the envelope function of the Wannier exciton wave function in reciprocal space (*14*, *27*). Thus, in the Wannier limit, where the wave functions of the constituent electrons are similar in nature as a function of $\mathbf{k}$, the probability of the XUV probe pulse photoemitting a constituent electron from the exciton with momentum $\mathbf{k}$ is proportional to $|A_\mathbf{k}|^2$. That is, the momentum-resolved intensity distribution of the photoemitted electrons in k-space directly images the modulus squared of the excitonic envelope function in reciprocal space, which we will refer to as simply the wave function squared. At finite temperatures, one needs to also consider the thermal occupation of excitons with finite center of mass (COM) momentum, which broadens the measured photoemission spectrum. However, our ab initio calculations show that this thermal broadening effect can be sufficiently small, for low enough temperatures. (fig. S4).

In our experiment, performed at 90 K, as we lower the exciton density by lowering the optical pump pulse intensity, we see a rapid reduction in the width of the measured k-space distribution, as broadening effects due to many-exciton interactions decrease (fig. S5). For densities of $<10^{12}$ cm^{-2}, one expects minimal exciton-exciton interactions since the average interexcitonic distance exceeds the expected (few nanometer) size of the exciton (*33*). Thus, the width of the ARPES peak approaches the intrinsic width of the exciton in k-space. Figure 2A and fig. S3 show the measured excitonic wave function squared at a total exciton density of ~1×10^{11} cm^{-2}, as recorded at a time delay of 0.5 ps. The choice of a nonzero delay ensures the absence of a signal from the transient Floquet-like state, which would otherwise coincide with the exciton signal for resonant excitation conditions at zero delay and thus complicate the measurement of the wave function. Beyond zero delay, we find that for the resonant, low-excitation conditions, the measured k-space distribution is largely unchanged as a function of time delay (fig. S6), suggesting that quasi-equilibrium conditions are rapidly achieved within our few hundred femtosecond temporal resolution. A calculation using first-principles GW-BSE techniques (*34*–*36*)

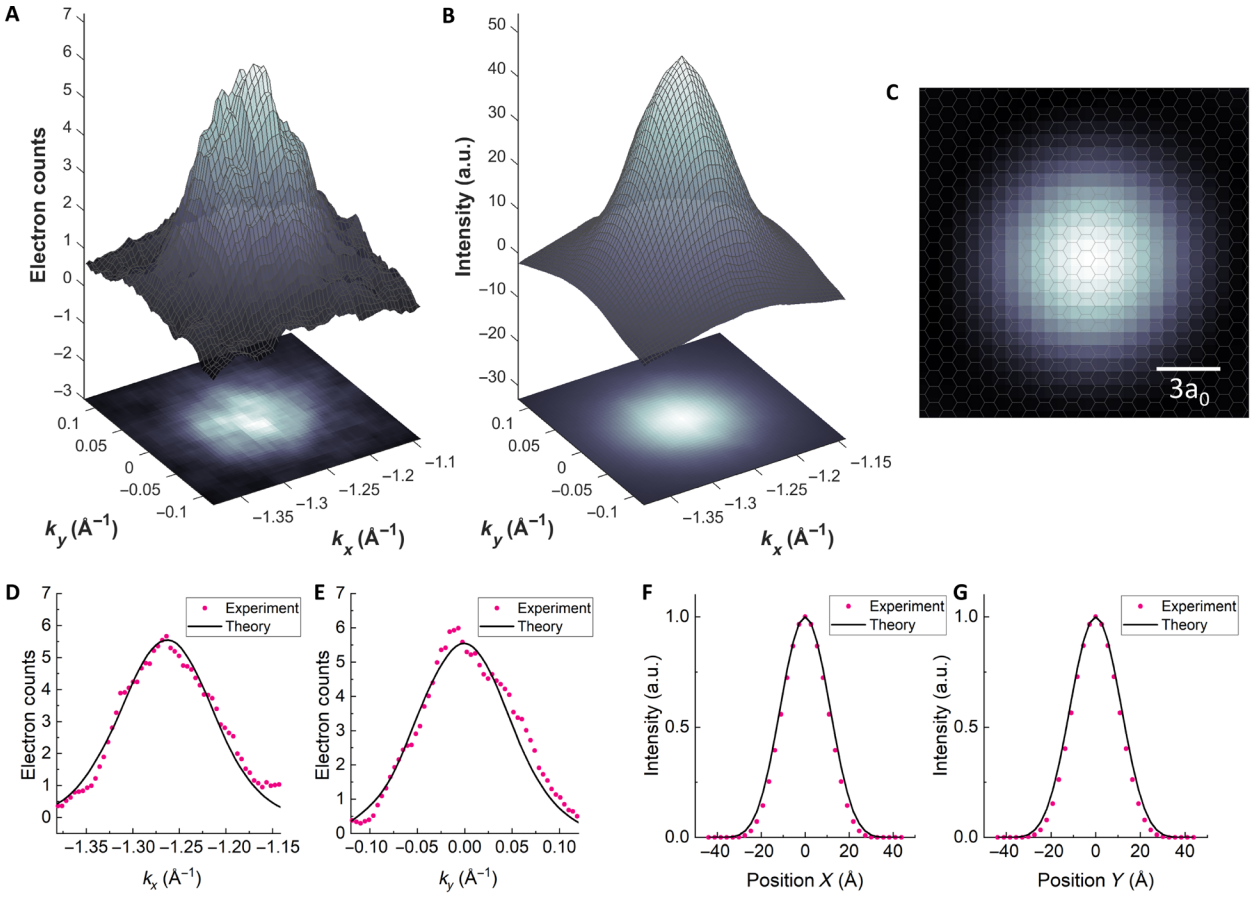

Fig. 2. Excitonic wave function squared of the K-valley exciton. (**A**) Experiment and (**B**) theory in momentum space. (**C**) Wave function squared in real space obtained by Fourier transform of the experimental data. The overlay of the WSe_2 lattice shows the relative electron-hole distances extend over many lattice sites—the hallmark of a Wannier-type exciton. (**D** to **G**) Profile comparisons of experiment and theory in two orthogonal directions in momentum (D and E) and real space (F and G).

reproduces the measured excitonic wave function in the full 2D reciprocal space very well (Fig. 2, B, D, and E). From our measurements, we obtain a root mean square (RMS) radius in *k*-space of 0.072 1/Å, which corresponds to an RMS radius of 1.4 nm in real space (Fig. 2C and see Supplementary Text for details), in excellent agreement with our theory (Fig. 2, F and G). Previous magneto-optical studies on WSe_2 have reported a radius of 1.7 nm (RMS) for encapsulated samples, where a slightly larger radius is expected because of the increased dielectric screening from the encapsulating hBN layers (*33*). As discussed previously, the finite temperature of 90 K in our experiments gives rise to an extra broadening in *k*-space from the thermal distribution of the exciton COM wave vector Q. Ab initio calculations show that, for these tightly bound excitons, the contribution of the thermal broadening is less than 10% (fig. S4), which is within our experimental and theoretical uncertainties.

Besides the momentum resolution of the wave function, our experiments also allow us to resolve the energy of the photoemitted electron (Fig. 3) and, thus, measure the dispersion relation of electrons originating from excitons. Under our low-temperature and low-density conditions, we have the opportunity to evaluate the predicted anomalous dispersion (*27*, *28*, *30*), a signature of excitons that has been elusive in experimental studies performed under different conditions (*30*, *31*). On the basis of momentum and energy conservation, one can show that electrons bound to holes in excitons, upon being photoemitted, will exhibit a negative energy-momentum dispersion relationship that resembles the VB of the hole (see Supplementary Text for a detailed description of the phenomenon).

In Fig. 3B, we plot the energy-momentum distribution of the photoemitted electron versus *k* along the K-Γ direction of the Brillouin zone (BZ). For each *k*, we see a distribution in the measured photoelectron energies (Fig. 3C), which is largely due to the inhomogeneous broadening in the photoemission signal from our sample. Despite this energy distribution, one clearly sees the negative dispersion exhibited by the photoemitted electron. To analyze this further, we extract the peak energy of the distribution for every point in the 2D *k*-space (Fig. 3A, yellow surface, and see Supplementary Text for details). A similar analysis is also performed for the VB, thus providing its dispersion over the 2D *k*-space as well (Fig. 3A, blue surface). Together, they exhibit a notable visual of the negative curvature of the VB and the subgap excitonic signal. We also note that Fig. 3A provides a remarkable illustration of how an ARPES-based measurement encodes a correlated two-particle state in a single-particle band structure. In Fig. 3B, we plot the peak energy versus *k* for the exciton (magenta line) and the VB (dashed yellow), showing the comparable negative curvatures of the two signals in an overlay (the VB is displaced in energy for an easier comparison). We expect

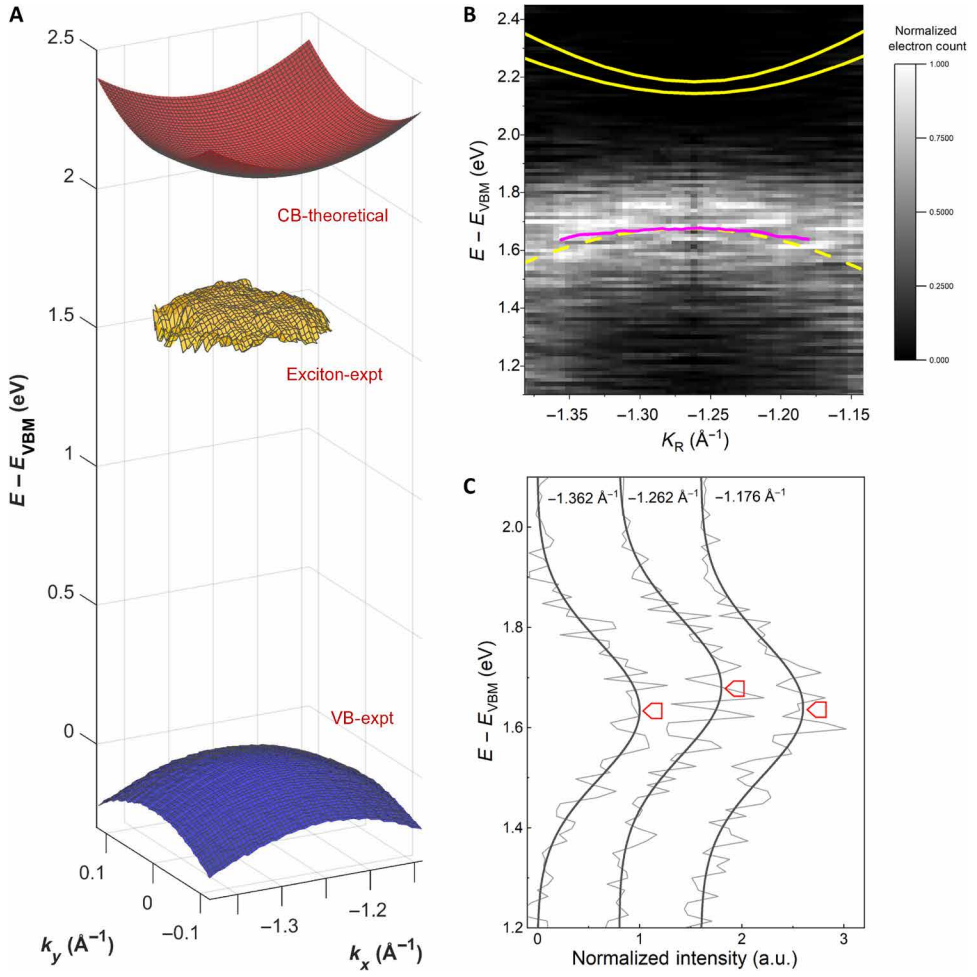

Fig. 3. Anomalous negative dispersion of the electron photoemitted from an exciton. (**A**) Measured energy-momentum dispersion relationship over the 2D *k*-space for the electron photoemitted from the exciton and from the VB. Notably, the exciton signal shows a negative dispersion resembling the VB. A theory calculation for the dispersion of the conduction band (CB) is also shown for comparison. The dispersion relationship for the exciton (yellow) and VB (blue) are obtained by fitting the experimental energy distribution curves and extracting their peak values $E_X(\mathbf{k})$ and $E_{VB}(\mathbf{k})$ at each momentum. (see Supplementary Text) (**B**) Measured energy-momentum distribution of the electrons photoemitted from an exciton, along a 1D cut in *k*-space centered at the K-valley. For each value of $k_{||}$, the intensity versus the energy is normalized to its maximum value. The yellow solid curves are the theoretical spin-split CBs. The dashed yellow and magenta curves correspond to $E_{VB}(\mathbf{k})$ and $E_X(\mathbf{k})$, with $E_{VB}(\mathbf{k})$ offset in its energy position for easy comparison to $E_X(\mathbf{k})$. (**C**) Energy distribution curves (light gray) and Gaussian fitting (black) for three representative values of $k_{||}$ from (B), with red ⌓ symbol marking the peak positions of the fitted curve.

any discrepancy to reflect experimental uncertainty, inhomogeneous broadening in the photoemission signal of the sample and finite temperature effects. We also note that our measurements were performed at a nonzero delay to ensure that the observed negative dispersion feature is not due to the sideband replica of the VB, related to the transient Floquet-like state, which is present only for zero delay.

DISCUSSION

Our experiments of photodissociating the exciton and measuring the photoemitted electron distribution in energy and momentum spaces allow for unprecedented information about excitons. In the immediate future, one could image the wave function of other interesting excitonic states, such as the momentum- or spin-forbidden dark excitons or the p-like excited states. Similar studies in other interesting material systems, such as the transition metal dichalcogenide hetero- and homobilayers, 2D perovskites, could provide a rich understanding of exciton physics therein. Furthermore, it is likely that the central idea of dissociating composite quasiparticles and measuring their constituents via TR-ARPES could be extended to study other optically excited states, such as trions and biexcitons. Beside accessing steady-state properties of these particles, our time and momentum resolution could also access their coherent dynamics and transient phenomena over the full BZ (*29*), an intriguing future avenue of investigation. Furthermore, our current use of low-intensity above-gap excitation, or future integration with intense below band-gap pump pulses, which minimizes heating and other detrimental effects, would enable the observation of emergent phenomena in quantum materials. In general, these studies are of great topical interest, with powerful new techniques being developed to realize these goals (*37*–*39*). In this context, from the point of view of

excitons, our work raises the intriguing question of whether these studies from an ensemble of excitons could reveal the nature of emerging equilibrium and nonequilibrium many-exciton states that form after photoexcitation.

MATERIALS AND METHODS

Sample preparation

WSe_2 and hBN were mechanically exfoliated and stacked onto an n-doped Si substrate by dry-transfer technique. Size of the ML WSe_2 is around 40 μm by 20 μm. The hBN buffer is around 20 nm in thickness, this buffer layer provides a clean and flat support, and it also provides a dielectric environment that prevents quenching of exciton. The ML WSe_2 was connected to bulk WSe_2 that sits directly on top of the Si substrate, and this provides a conductive pathway and prevents sample charging. More details about the sample preparation and geometry can be found in (*29*).

Optical pump and XUV probe

Our optical setup has been described in detail previously (*29*). The optical pump and probe are driven by an ytterbium-doped fiber amplifiers laser system that operates at 2 MHz, providing 230-fs pulses at 1030 nm and a pulse energy of 100 μJ. Twenty microjoules of this pump is used to drive a noncollinear optical parametric amplifier (NOPA), which provides a tunable wavelength from 320 to 2500 nm with a 5-nm spectral bandwidth and with pulse energies ranging from 0.1 to 1 μJ. We use the output of this NOPA to photoexcite the sample, and an incident angle is 68° from surface normal. For the low-temperature experiment, we photoexcite the sample resonantly at 1.72 eV (with 5-nm bandwidth) with a photoexcitation density of $1.02 \times 10^{11}/cm^2$. Details about estimating the photoexcitation density are provided in Supplementary Text.

For the XUV probe, with a beta-barium borate (BBO) crystal, we frequency doubled 30 μJ of 1030 nm from the laser system generating 14 μJ of 515-nm radiation. High harmonic generation is performed by focusing the 515-nm beam into a Kr gas jet in vacuum, reaching a power density of 3×10^{14} W/cm^2. Of the different harmonics, 21.7-eV photon was selected by a combination of Al and Sn filters. In all the experiments, the probe pulse was p-polarized, and its incident angle on the sample is 68° from surface normal. The effective temporal resolution of this pump-probe setup was ~240 fs.

Time-resolved angle-resolved photoemission spectroscopy

TR-ARPES was performed in a time-of-flight momentum microscope (*29*). Photoelectrons emitted from the sample were collected by an immersion objective lens, providing access to full half-space above the sample surface. A field aperture inserted at the Gaussian image plane of the electron optics was used to selectively allow only electrons emitted from the ML region of the sample to pass through. Momentum-space (ARPES) image of this selected sample area was obtained by imaging the back focal plane of the objective lens, and energy-resolved spectrum was measured by a time-of-flight detector. Energy resolution of the instrument was determined by the drift energy of electrons in the time-of-flight drift tube, and in this experiment, the effective energy resolution was set to 30 meV.

First-principles calculations

Density functional calculations within the local density approximation (LDA) were performed using the Quantum ESPRESSO package (*40*). We used the experimental lattice constant of 3.28 Å in our calculations. The GW (*34*) calculations were carried out using the BerkeleyGW package (*36*). In the calculation of the electron self-energy, the dielectric matrix was constructed with a cutoff energy of 35 rydbergs. The dielectric matrix and the self-energy were calculated on an 18 by 18 by 1 *k*-grid. The quasiparticle bandgap was converged to within 0.05 eV. The spin-orbit coupling was included perturbatively within the LDA formalism. The calculations of the excitonic ARPES spectra use ensemble average of photoelectrons emitted from excitons of different momenta, with the exciton population following quasi-equilibrium Boltzmann distribution in the K-valley. The exciton energy levels and wave function are calculated using the GW-BSE methods implemented in the BerkeleyGW package, with the *k*-grid sampled in the K-valleys and the grid density equivalent to 14,400 points in the first Brillouin zone (*35*). In general, the GW-BSE method is expected to be accurate to within roughly 100 meV for quasiparticle bandgaps of semiconductors (*41*). Another important consideration is the convergence parameters coming from the number of *k*-points, number of empty bands, and dielectric cutoff, which, in our case, yield an error smaller than 50 meV. The calculated energy levels of K-valley excitons can be further affected by factors such as the choice of lattice constant and the pseudo-potential used in the calculations.

SUPPLEMENTARY MATERIALS

Supplementary material for this article is available at http://advances.sciencemag.org/cgi/content/full/7/17/eabg0192/DC1

REFERENCES AND NOTES

1. J. Frenkel, On the transformation of light into heat in solids. I. *Phys. Rev.* **37**, 17–44 (1931).
2. G. H. Wannier, The structure of electronic excitation levels in insulating crystals. *Phys. Rev.* **52**, 191–197 (1937).
3. R. Peierls, Zur Theorie der Absorptionsspektren fester Körper. *Ann. Phys.* **405**, 905–952 (1932).
4. N. F. Mott, Conduction in polar crystals. II. The conduction band and ultra-violet absorption of alkali-halide crystals. *Trans. Faraday Soc.* **34**, 500–506 (1938).
5. W. Kohn, D. Sherrington, Two kinds of bosons and bose condensates. *Rev. Mod. Phys.* **42**, 1–11 (1970).
6. J. P. Eisenstein, Exciton condensation in bilayer quantum hall systems. *Annu. Rev. Condens. Matter Phys.* **5**, 159–181 (2014).
7. D. Snoke, Spontaneous Bose coherence of excitons and polaritons. *Science* **298**, 1368–1372 (2002).
8. D. Jérome, T. M. Rice, W. Kohn, Excitonic insulator. *Phys. Rev.* **158**, 462–475 (1967).
9. S. T. Omelchenko, Y. Tolstova, H. A. Atwater, N. S. Lewis, Excitonic effects in emerging photovoltaic materials: A case study in Cu_2O. *ACS Energy Lett.* **2**, 431–437 (2017).
10. V. D'Innocenzo, G. Grancini, M. J. P. Alcocer, A. R. S. Kandada, S. D. Stranks, M. M. Lee, G. Lanzani, H. J. Snaith, A. Petrozza, Excitons versus free charges in organo-lead tri-halide perovskites. *Nat. Commun.* **5**, 3586 (2014).
11. D. Marongiu, M. Saba, F. Quochi, A. Mura, G. Bongiovanni, The role of excitons in 3D and 2D lead halide perovskites. *J. Mater. Chem. C.* **7**, 12006–12018 (2019).
12. F. Li, L. Yang, Z. Cai, K. Wei, F. Lin, J. You, T. Jiang, Y. Wang, X. Chen, Enhancing exciton binding energy and photoluminescence of formamidinium lead bromide by reducing its dimensions to 2D nanoplates for producing efficient light emitting diodes. *Nanoscale* **10**, 20611–20617 (2018).
13. T. Mueller, E. Malic, Exciton physics and device application of two-dimensional transition metal dichalcogenide semiconductors. *npj 2D Mater. Appl.* **2**, 29 (2018).
14. G. Dresselhaus, Effective mass approximation for excitons. *J. Phys. Chem. Solid* **1**, 14–22 (1956).
15. G. Dresselhaus, Absorption coefficients for exciton absorption lines. *Phys. Rev.* **106**, 76–78 (1957).
16. J. Shah, *Ultrafast Spectroscopy of Semiconductors and Semiconductor Nanostructures* (Springer Series in Solid-State Sciences, Springer Berlin Heidelberg, 1999), vol. 115.
17. H. Ohnishi, N. Tomita, K. Nasu, Direct determination of exciton wavefunction amplitudes by the momentum-resolved photo-electron emission experiment. *Int. J. Mod. Phys. B.* **32**, 1850094 (2018).

18. K. F. Mak, C. Lee, J. Hone, J. Shan, T. F. Heinz, Atomically thin MoS_2: A new direct-gap semiconductor. *Phys. Rev. Lett.* **105**, 136805 (2010).
19. A. Splendiani, L. Sun, Y. Zhang, T. Li, J. Kim, C. Y. Chim, G. Galli, F. Wang, Emerging photoluminescence in monolayer MoS_2. *Nano Lett.* **10**, 1271–1275 (2010).
20. S. Das, J. A. Robinson, M. Dubey, H. Terrones, M. Terrones, Beyond graphene: Progress in novel two-dimensional materials and van der waals solids. *Annu. Rev. Mat. Res.* **45**, 1–27 (2015).
21. M. Puppin, Y. Deng, C. W. Nicholson, J. Feldl, N. B. M. Schröter, H. Vita, P. S. Kirchmann, C. Monney, L. Rettig, M. Wolf, R. Ernstorfer, Time- and angle-resolved photoemission spectroscopy of solids in the extreme ultraviolet at 500 kHz repetition rate. *Rev. Sci. Instrum.* **90**, 023104 (2019).
22. A. K. Mills, S. Zhdanovich, M. X. Na, F. Boschini, E. Razzoli, M. Michiardi, A. Sheyerman, M. Schneider, T. J. Hammond, V. Süss, C. Felser, A. Damascelli, D. J. Jones, Cavity-enhanced high harmonic generation for extreme ultraviolet time- and angle-resolved photoemission spectroscopy. *Rev. Sci. Instrum.* **90**, 083001 (2019).
23. B. Krömker, M. Escher, D. Funnemann, D. Hartung, H. Engelhard, J. Kirschner, Development of a momentum microscope for time resolved band structure imaging. *Rev. Sci. Instrum.* **79**, 053702 (2008).
24. K. Medjanik, O. Fedchenko, S. Chernov, D. Kutnyakhov, M. Ellguth, A. Oelsner, B. Schönhense, T. R. F. Peixoto, P. Lutz, C.-H. Min, F. Reinert, S. Däster, Y. Acremann, J. Viefhaus, W. Wurth, H. J. Elmers, G. Schönhense, Direct 3D mapping of the Fermi surface and Fermi velocity. *Nat. Mater.* **16**, 615–621 (2017).
25. A. Steinhoff, M. Florian, M. Rösner, G. Schönhoff, T. O. Wehling, F. Jahnke, Exciton fission in monolayer transition metal dichalcogenide semiconductors. *Nat. Commun.* **8**, 1166 (2017).
26. E. Perfetto, D. Sangalli, A. Marini, G. Stefanucci, First-principles approach to excitons in time-resolved and angle-resolved photoemission spectra. *Phys. Rev. B* **94**, 245303 (2016).
27. A. Rustagi, A. F. Kemper, Photoemission signature of excitons. *Phys. Rev. B* **97**, 235310 (2018).
28. D. Christiansen, M. Selig, E. Malic, R. Ernstorfer, A. Knorr, Theory of exciton dynamics in time-resolved ARPES: Intra- and intervalley scattering in two-dimensional semiconductors. *Phys. Rev. B* **100**, 205401 (2019).
29. J. Madéo, M. K. L. Man, C. Sahoo, M. Campbell, V. Pareek, E. L. Wong, A. Al-Mahboob, N. S. Chan, A. Karmakar, B. M. K. Mariserla, X. Li, T. F. Heinz, T. Cao, K. M. Dani, Directly visualizing the momentum-forbidden dark excitons and their dynamics in atomically thin semiconductors. *Science* **370**, 1199–1204 (2020).
30. M. Weinelt, M. Kutschera, T. Fauster, M. Rohlfing, Dynamics of exciton formation at the Si(100) c(4 × 2) surface. *Phys. Rev. Lett.* **92**, 126801 (2004).
31. X. Cui, C. Wang, A. Argondizzo, S. Garrett-Roe, B. Gumhalter, H. Petek, Transient excitons at metal surfaces. *Nat. Phys.* **10**, 505–509 (2014).
32. M. K. L. Man, S. Deckoff-Jones, A. Winchester, G. S. Shi, G. Gupta, A. D. Mohite, S. Kar, E. Kioupakis, S. Talapatra, K. M. Dani, Protecting the properties of monolayer MoS_2 on silicon based substrates with an atomically thin buffer. *Sci. Rep.* **6**, 20890 (2016).
33. A. V. Stier, N. P. Wilson, K. A. Velizhanin, J. Kono, X. Xu, S. A. Crooker, Magnetooptics of exciton rydberg states in a monolayer semiconductor. *Phys. Rev. Lett.* **120**, 057405 (2018).
34. M. S. Hybertsen, S. G. Louie, Electron correlation in semiconductors and insulators: Band gaps and quasiparticle energies. *Phys. Rev. B* **34**, 5390–5413 (1986).
35. M. Rohlfing, S. G. Louie, Electron-hole excitations and optical spectra from first principles. *Phys. Rev. B* **62**, 4927–4944 (2000).
36. J. Deslippe, G. Samsonidze, D. A. Strubbe, M. Jain, M. L. Cohen, S. G. Louie, BerkeleyGW: A massively parallel computer package for the calculation of the quasiparticle and optical properties of materials and nanostructures. *Comput. Phys. Commun.* **183**, 1269–1289 (2012).
37. M. Borsch, C. P. Schmid, L. Weigl, S. Schlauderer, N. Hofmann, C. Lange, J. T. Steiner, S. W. Koch, R. Huber, M. Kira, Super-resolution lightwave tomography of electronic bands in quantum materials. *Science* **370**, 1204–1207 (2020).
38. L. Luo, X. Yang, X. Liu, Z. Liu, C. Vaswani, D. Cheng, M. Mootz, X. Zhao, Y. Yao, C.-Z. Wang, K.-M. Ho, I. E. Perakis, M. Dobrowolska, J. K. Furdyna, J. Wang, Ultrafast manipulation of topologically enhanced surface transport driven by mid-infrared and terahertz pulses in Bi_2Se_3. *Nat. Commun.* **10**, 607 (2019).
39. X. Yang, C. Vaswani, C. Sundahl, M. Mootz, L. Luo, J. H. Kang, I. E. Perakis, C. B. Eom, J. Wang, Lightwave-driven gapless superconductivity and forbidden quantum beats by terahertz symmetry breaking. *Nat. Photonics* **13**, 707–713 (2019).
40. P. Giannozzi, S. Baroni, N. Bonini, M. Calandra, R. Car, C. Cavazzoni, D. Ceresoli, G. L. Chiarotti, M. Cococcioni, I. Dabo, A. D. Corso, S. De Gironcoli, S. Fabris, G. Fratesi, R. Gebauer, U. Gerstmann, C. Gougoussis, A. Kokalj, M. Lazzeri, L. Martin-Samos, N. Marzari, F. Mauri, R. Mazzarello, S. Paolini, A. Pasquarello, L. Paulatto, C. Sbraccia, S. Scandolo, G. Sclauzero, A. P. Seitsonen, A. Smogunov, P. Umari, R. M. Wentzcovitch, Quantum ESPRESSO: A modular and open-source software project for quantum simulations of materials. *J. Phys. Condens. Matter* **21**, 395502 (2009).
41. S. G. Louie, *Topics in Computational Materials Science* (WORLD SCIENTIFIC, 1998); www.worldscientific.com/worldscibooks/10.1142/3487.
42. A. Damascelli, Probing the electronic structure of complex systems by ARPES. *Phys. Scr.* **T109**, 61–74 (2004).

Acknowledgments

Funding: This work was supported in part by JSPS Kakenhi grant number JP17K04995 and the Kick-start fund KICKS, Okinawa Institute of Science and Technology Graduate University. Funding was also provided in part by the Femtosecond Spectroscopy Unit of the Okinawa Institute of Science and Technology Graduate University. We thank OIST engineering support section for support. This research (theoretical analysis and first-principles calculations) was partially supported by NSF through the University of Washington Materials Research Science and Engineering Center DMR-1719797. Research at SLAC was supported by the AMOS program, Chemical Sciences, Geosciences, and Biosciences Division, Basic Energy Sciences, U.S. Department of Energy under contract DE-AC02-76-SF00515. T.C. acknowledges support from the Micron Foundation and a GLAM postdoctoral fellowship at Stanford. K.X. acknowledges support by the state of Washington through the University of Washington Clean Energy Institute. Computational resources were provided by Hyak at UW and the Extreme Science and Engineering Discovery Environment (XSEDE), which is supported by NSF under grant no. ACI-1053575. The work of M.C. and X.L. at Austin was partially supported by the NSF through the Center for Dynamics and Control of Materials: an NSF MRSEC under cooperative agreement no. DMR-1720595 and the facility supported by the center. **Author contributions:** M.K.L.M., J.M., C.S., EL.W., V.P., and A.A.-M. performed the experiments with assistance from D.R.B., M.M.M.A., and X.Z. M.K.L.M., K.M.D., J.M., and N.S.C. analyzed the data. M.C. and X.L. prepared the sample. V.P. and A.K. characterized the sample. T.C., F.H.d.J., and T.F.H. provided the theoretical support. K.X. and T.C. performed first principle theoretical calculations with help from F.H.d.J. K.M.D. and T.C. conceived the experiment. K.M.D. supervised the project. All authors contributed to discussions and manuscript preparation. **Competing interests:** J.M., M.K.L.M., and K.M.D. are inventors on a provisional patent application related to this work filed by the Okinawa Institute of Science and Technology School Corporation (no. US 2020/0333559 A1, filed on 16 April 2019, and published on 22 October 2020). The authors declare that they have no other competing interests. **Data and materials availability:** All data needed to evaluate the conclusions in the paper are present in the paper and/or the Supplementary Materials. Additional data related to this paper may be requested from the corresponding author.

Submitted 5 December 2020
Accepted 4 March 2021
Published 21 April 2021
10.1126/sciadv.abg0192

Citation: M. K. L. Man, J. Madéo, C. Sahoo, K. Xie, M. Campbell, V. Pareek, A. Karmakar, E L. Wong, A. Al-Mahboob, N. S. Chan, D. R. Bacon, X. Zhu, M. M. M. Abdelrasoul, X. Li, T. F. Heinz, F. H. da Jornada, T. Cao, K. M. Dani, Experimental measurement of the intrinsic excitonic wave function. *Sci. Adv.* **7**, eabg0192 (2021).

Experimental measurement of the intrinsic excitonic wave function

Michael K. L. Man, Julien Madéo, Chakradhar Sahoo, Kaichen Xie, Marshall Campbell, Vivek Pareek, Arka Karmakar, E Laine Wong, Abdullah Al-Mahboob, Nicholas S. Chan, David R. Bacon, Xing Zhu, Mohamed M. M. Abdelrasoul, Xiaoqin Li, Tony F. Heinz, Felipe H. da Jornada, Ting Cao and Keshav M. Dani

Sci Adv **7** (17), eabg0192.
DOI: 10.1126/sciadv.abg0192